

Estimating MIMO Capacities from Broadband Measurements in a Cellular Network

S. Jaeckel and V. Jungnickel

Fraunhofer Inst. for Telecommunications,

Heinrich Hertz Institute, 10587 Berlin, Germany

eMail: { stephan.jaeckel ; volker.jungnickel }@hhi.fraunhofer.de

Abstract—We provide a new efficient method to evaluate spectral efficiencies from wireless channel soundings. Measurements are done in a limited cellular network using 3 sites with an ISD of 750 m. Each site has 3 sectors and is equipped with cross-polarized panel antennas. In the preprocessing phase, we take advantage of the high number of elements at the measurement array to compute a virtual cross polarized 2x2 setup with omnidirectional coverage at the receiver. We then apply findings from the mid 1990s to denoise the data by an adaptive thresholding method. This approach gains roughly 10 dB of SNR and enables us to evaluate capacities also for well shaded locations with a high path loss. At a fixed evaluation SNR of 10 dB, our setup achieves 5.7 bps/Hz which compares well to earlier findings from Manhattan. Exploiting both effects, the received power and the structure of the MIMO channel, best server capacities are calculated to 15 bps/Hz while the corresponding SISO setup only achieves 7.6 bps/Hz.

I. INTRODUCTION

Information theory predicts significant gains in capacity by using multiple antennas at the transmitter and at the receiver [1]. Current systems such as 3GPP LTE and Wimax will take advantage of multiple antennas, but it is important to gain knowledge about the achievable performance under real world deployment and interference conditions. This is normally done by system level simulations. The calibration of those simulation environments often relies on channel measurements to estimate necessary parameters and setups.

One parameter, the multiple-input multiple-output (MIMO) capacity, describes the maximal achievable throughput of the multi antenna communication channel. Unfortunately, it is difficult to compute from measured data because of the noise. Capacity measurements in outdoor scenarios thus often need complicated calibration and testing. Scenarios are often limited to narrowband soundings [2] where it is easy to achieve a high transmit power or stationary setups [3] where several successive measures can be averaged. Another method applies preprocessing techniques such as ESPRIT or Rimax [4] to determine the departure- and arrival angles of the signal paths. This information can then be used to reassemble channel matrices based on the estimated paths - at the cost of a high computational burden such that a statistical evaluation is hardly possible.

Our objective is to provide a more efficient method to estimate MIMO capacities from wireless channel measurements. Our approach first takes advantage of a higher number of antennas during the measurement by a simple linear weighting

and summation procedures. Within limits, this step can also approximate a great number of beam patterns for commercial antennas. We then apply findings from the mid 1990s to denoise the data by an adaptive thresholding method. This method gains enough signal to noise ratio (SNR) to evaluate capacities also for well shaded locations with a high path loss. We then calculate 2x2 MIMO capacities from a measurement campaign in the city area of Dresden (Germany) and compare our results with findings from Chizhik et al. [2].

II. EXPERIMENTAL SETUP

The measurement area is situated in the center of the city of Dresden. Fig. 2 shows the measurement track, the locations of the three base stations (BSs) with an inter-site distance (ISD) of 750 m and the sector orientations. All BSs operate at 0° downtilt during our measurement. A high precision odometer and a GPS receiver record the position of each snapshot. We cluster the snapshots along the 8.8 km measurement track in 2240 points with a diameter of 33λ to increase the precision of the results.

A HyEff channel sounder [5] records the radio channel with a bandwidth of 21.25 MHz at around 2.53 GHz by applying a multi-tone test signal with a duration of $12.8 \mu\text{s}$. We thus estimate the frequency response (FR) of the channel on 273 equidistantly spaced carriers. The single measurement chain of the sounder is consecutively switched to all transmit (Tx) and receive (Rx) antenna elements with the radio channel in between. Snapshot rates and recording times fulfill the channel sampling theorem. At the BS, we use pre-commercial +18 dBi antennas (Kathrein 80010541) with two cross-polarized ports $\pm 45^\circ$ (see Fig. 1). All sector antennas at one site are fed like a single cross-polarized array with six input ports in the same switching sequence. At the receiver, we use a polarized



Figure 1. Transmit antenna (left) and receive antenna (right)

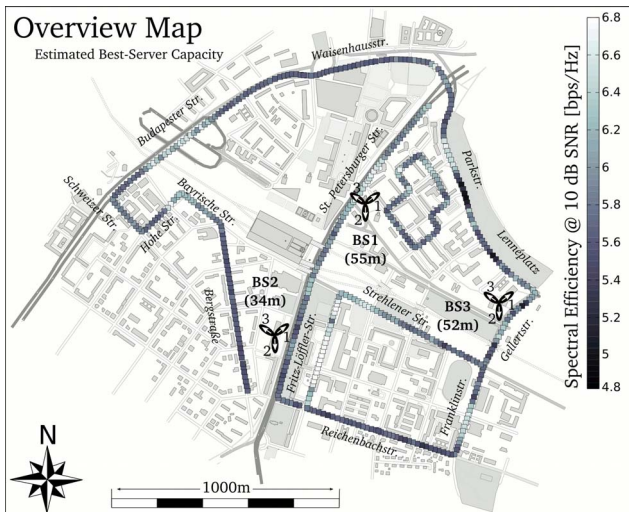


Figure 2. Overview map of the measurement area showing the positions and heights of the BSs, the sector orientations as black leaves and the estimated best server capacities for $\sigma=10$ dB along the measurement track.

uniform circular array (PUCA) with 8 patch elements [5]. Measurements with the same sounder but at other frequencies and with other antennas are also reported in [3–6]. Further details for this measurement campaign and additional results can be found in an earlier paper [6].

III. DATA PROCESSING

A detailed description of the data processing routine can be found in the appendix. Its basic components are the approximation of an omnidirectional antenna pattern (Appendix A) and the denoising procedure (Appendix B). In the first step, we measure the beam patterns of the 16-port receive antenna and calculate two sets of weights, one for the vertical and one for the horizontal polarization. Those weights enable us to combine the measured channel coefficients to

$$\hat{\mathbf{H}} = \sum_{r=1}^{16} \begin{pmatrix} \mathbf{w}_r^{(V)} \mathbf{h}_r \\ \mathbf{w}_r^{(H)} \mathbf{h}_r \end{pmatrix} \quad (1)$$

The virtual 2-port antenna separates both polarizations with more than 20 dB decoupling and the shape of its pattern is similar to the pattern of a dipole antenna. In the second step we first extract the taps by using an adaptive thresholding approach. Then, we reassemble a noise reduced version of the channel using those taps. Donoho and Johnstone [7, 8] discovered that an ideal reconstruction of the channel is achieved when there are less taps than carriers in the data (sparse channel) and when we use only taps above a certain threshold for the reconstruction. A detailed test with a simulated Keyhole channel based on Rayleigh fading shows that the estimation and reconstruction gains approx. 10 dB of SNR in our scenario (see Appendix D).

Using the denoised channels, we calculate the spectral efficiency C measured in units of bps/Hz (also called capacity) on each subcarrier n by a Singular Value Decomposition (SVD) of the channel matrix $\mathbf{H}_n = \mathbf{U}_n \mathbf{D}_n \mathbf{V}_n^H$. The diagonal matrix \mathbf{D}_n contains at most $n_\lambda = \min(n_t, n_r)$ nonzero singular

values λ . We compute the channel capacity as

$$C = \frac{1}{N} \sum_{n=1}^N \sum_{i=1}^{n_\lambda} \log_2 \left(1 + \frac{\sigma}{n_t \cdot \eta} \lambda_{i,n}^2 \right) \quad (2)$$

with η as the average path gain

$$\eta = \frac{1}{n_r n_t N} \sum_{r=1}^{n_r} \sum_{t=1}^{n_t} \sum_{n=1}^N |\mathbf{H}_{r,t,n}|^2 \quad (3)$$

Singular value statistics (as in Fig. 3, right) are calculated from normalized channel matrices where the effect of the fast fading has been averaged out before.

IV. RESULTS

The 2x2 MIMO capacity is calculated for a fixed SNR of 10 dB. Thus, the results depend only on the structure of the channel matrix and the received power has no influence. All 9575 locations where the measured SNR is above 5 dB are included in this study and we ensure that the potential capacity increase from noise is less than 10%. Results are depicted in Fig. 3. The median capacity is 5.7 bps/Hz. This result is very close to findings from Chizhik et al. [2] where capacities of 5.5 bps/Hz are estimated from a narrowband measurement. Distributions of the singular values (SVs) indicate that the measured channel matrix is better conditioned than the 2x2 Rayleigh i.i.d. channel. This can be attributed to the use of cross-polarized antennas. All areas showing high capacities above 6.5 bps/Hz in the map (Fig. 2) are served by line of sight (LOS). Note that 2x2 capacities at 10 dB SNR can have values in between 4 (fully singular matrices with only one nonzero SV) and 6.9 bps/Hz (fully orthogonal with equal SVs). LOS coverage thus provides the highest multiplexing gains for cross-polarized arrays.

The maximum throughput is achieved when including both, the effect of the received power and the structure of the channel matrix. The estimated spectral efficiency at the raw measurement SNR is depicted in Fig. 4. The figure shows the 2x2 MIMO capacity (black solid upper line) which is always more than twice as high as the corresponding single-input single-output (SISO) capacity (blue solid lower line). The dashed thin lines show the upper (orthogonal) and lower (singular) bound for the 2x2 MIMO capacity. One can observe that with our setup, the estimated capacities are always above 90% of the maximum value.

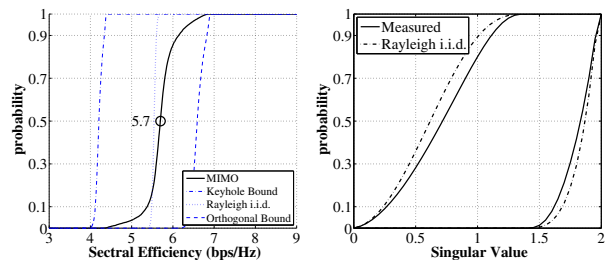


Figure 3. CDF of the capacity (left) and singular value distribution (right). Capacity distributions are given for the measured channels, as well as for the lower and upper bound.

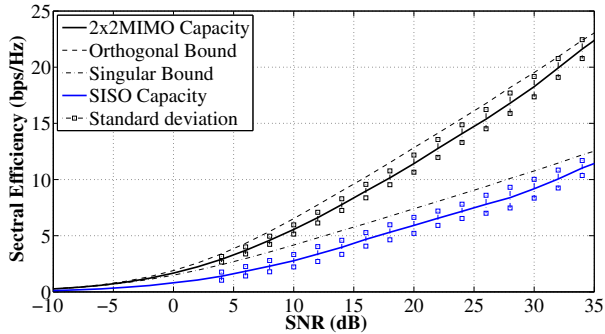


Figure 4. Estimated 2x2 MIMO capacities at the measurement SNR.

With the 2x2 cross polarized MIMO setup, best server capacities (median 15 bps/Hz) are about twice as high as the corresponding SISO capacities (median 7.6 bps/Hz). The estimated capacities are at least as high as the corresponding capacity of the i.i.d. channel at the same SNR. Thus, 2x2 MIMO with cross-polarized antennas can realize the gains predicted by theory. Note that these results apply only for the interference free link between one multi-antenna BS and one multi-antenna terminal.

V. SUMMARY AND DISCUSSION

We show that data processing can provide more detailed insights into the performance of cellular MIMO systems. Measurement antennas generally show better performance than antennas for commercial products. The beam patterns of those “real world” antennas can be approximated, provided that multi-element arrays are used for the measurement. Further processing of the measurement data can remove a significant part of the noise.

We use the processing output to estimate the broadband MIMO channel capacity for a mobile network. Our results confirm prior findings from narrowband measurements in Manhattan and we can provide reliable estimates also when the measurement SNR is low. We have generated statistics on the broadband capacity for large areas and at higher mobilities. Future work will focus on interference limited scenarios, higher numbers of antennas and the gains of BS cooperation in a statistical scenario.

APPENDIX

A. Antenna pattern shaping

The beam patterns of the receive array are measured in an anechoic chamber with one degree precision in azimuth and elevation. Two separate measurements are done for the horizontal and vertical polarization. We use a linear combination of each of the 16 elements of the receive array to emulate omnidirectional coverage. This gives more representative results and provides an additional array gain for the data evaluation. The linear weights are calculated separately for each polarization. We first assemble a matrix \mathbf{P} containing all measured patterns of the same polarization at 0 degree elevation. E.g. we get $\mathbf{P}^{(V)}$ with 8 rows, one for each patch element, and 360 columns representing the measured beam patterns where the Tx and

the Rx are aligned at vertical polarization. Likewise, we get $\mathbf{P}^{(H)}$ by using the patterns with horizontal alignment. In the second step, we calculate the Moore-Penrose pseudoinverse of $\mathbf{P}^{(V)}$ and $\mathbf{P}^{(H)}$

$$\mathbf{P}^{-1} = \mathbf{P}^H \cdot (\mathbf{P}\mathbf{P}^H)^{-1} \quad (4)$$

Now, we provide a new beam pattern with our desired shape. We want to emulate an omnidirectional 1x360 pattern given as a vector of ones. Note here, that theoretically any pattern can be approximated in this way. The approximation accuracy solely depends on the number of elements at the measurement antenna. The weights are now calculated by multiplying our desired pattern with \mathbf{P}^{-1}

$$\mathbf{w} = \underbrace{\left(\frac{1}{360n_r} \sum_{r=1}^{n_r} \sum_{\Phi=1}^{360} |\mathbf{P}_{r,\Phi}|^2 \right)^{-\frac{1}{2}}}_{\text{normalization}} \cdot \underbrace{(1 \ 1 \ \dots \ 1)}_{\text{desired pattern}} \cdot \mathbf{P}^{-1} \quad (5)$$

This calculation is done separately for both polarizations resulting in two weight vectors $\mathbf{w}^{(V)}$ and $\mathbf{w}^{(H)}$ for the vertical and horizontal alignment, respectively. In a last step, we apply the two weight vectors to the measured pattern at all azimuth and elevation angles to calculate the effective beam pattern of the virtual antenna.

B. Denoising by tap estimation

Both, the measured and the effective channel coefficients can be seen as

$$\mathbf{y}_n = \mathbf{h}_n + \mathbf{v}_n, \quad n \in \{1, 2, \dots, N\} \quad (6)$$

where \mathbf{y} is the observation of the broadband radio channel \mathbf{h} in frequency domain at N fixed pilot positions ν_n with $\nu_n \in \mathbb{R}$ and $0 \leq \nu_n < 1$. Note that the pilot positions do not need to be equidistant. \mathbf{v} is assumed to be additive white Gaussian noise (AWGN). We further assume that the FR of the channel can be modelled as a sum of discrete reflections (channel filter taps) of the transmitted waveform at obstacles in the physical environment [9]. We want to estimate the taps from the observation \mathbf{y} in an iterative fashion in order to find a representation $\hat{\mathbf{h}}$ of the channel where most of the noise has been removed. In each iteration step, we estimate the

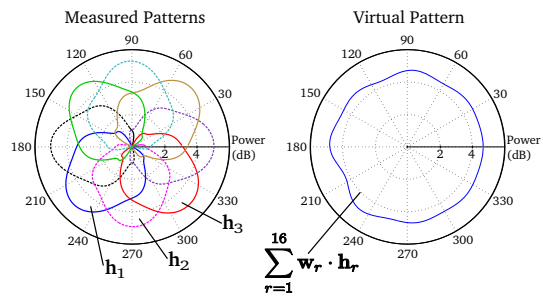


Figure 5. Measured and virtual V-V pattern at 0° elevation

normalized delay $m_l = \tau_l \cdot B$ of the l^{th} tap by

$$m_l = \arg \max_{m_l} \left| \sum_{n=1}^N \mathbf{g}_n \cdot e^{-2\pi j \cdot m_l \cdot \nu_n} \right| \quad (7)$$

For the first step we use $\mathbf{g}_n = \mathbf{y}_n$ from (6). $m_l \in \mathbb{R}$ can have values $0 \leq m_l < \tau_m \cdot B$ with τ_m as the maximum delay in the measurement. For the amplitude α_l and phase ϕ_l follows

$$\alpha_l \cdot e^{j\phi_l} = \frac{1}{N} \cdot \sum_{n=1}^N \mathbf{g}_n \cdot e^{-2\pi j \cdot m_l \cdot \nu_n} \quad (8)$$

In further iteration steps we can set \mathbf{g}_n in two ways:

1) We want to estimate a new tap and we know L taps already. Therefore we remove all previously detected taps from the observation \mathbf{y} .

$$\mathbf{g}_n^{(L+1)} = \mathbf{y}_n - \sum_{l=1}^L \alpha_l \cdot e^{j\phi_l} \cdot e^{-2\pi j \cdot m_l \cdot \nu_n} \quad (9)$$

2) The values α , ϕ and τ of each tap are distorted by interference from the following (undetected) taps and also by approximation errors of already estimated ones. After we estimated a new tap, we can thus increase the precision of a previously detected tap k by setting \mathbf{g} to

$$\mathbf{g}_n^{(k)} = \mathbf{y}_n - \sum_{\forall l \neq k} \alpha_l \cdot e^{j\phi_l} \cdot e^{-2\pi j \cdot m_l \cdot \nu_n} \quad (10)$$

and repeating the calculation for this tap. Candes and Tao [10] state that for a sparse \mathbf{h} , which is satisfied when there are less taps L than observations N , we can find a $\hat{\mathbf{h}}$ such that the mean square error (MSE) is within a factor of $\log N$ of the ideal MSE

$$\|\hat{\mathbf{h}} - \mathbf{y}\|^2 = O(\log N) \cdot \mathbb{E}\|\mathbf{y} - \mathbf{h}\|^2 \quad (11)$$

Donoho and Johnstone [7, 8] further state that thresholding achieves the ideal MSE with a threshold level at $\sqrt{2 \cdot \log N} \cdot \sigma$. In general, the exact number of taps is unknown. We can gain knowledge about the noise power P_N , and thus the threshold from the link budget in the measurement setup. Nevertheless, if the exact value P_N is also unknown and we can certify that $L \ll N$, then we can set the threshold in an adaptive fashion.

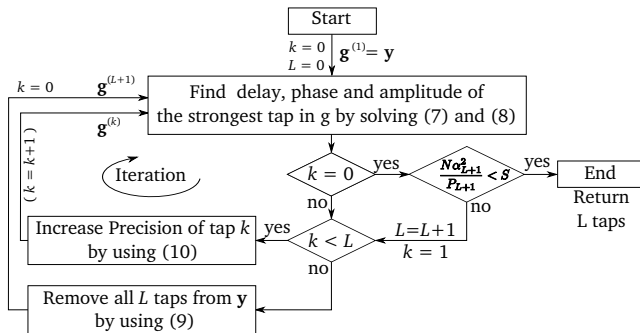


Figure 6. Flow chart of the iterative tap detection with adaptive thresholding. The inner iteration loop can be repeated more than once for each new detected tap - resulting in further precision improvements.

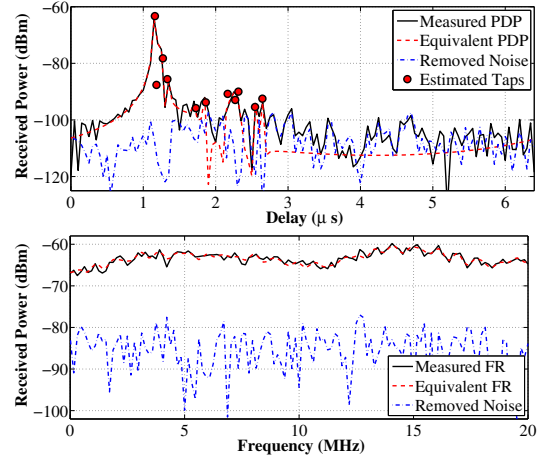


Figure 7. Example output of the iterative tap estimation in the time domain (top) and frequency domain (bottom). The measured channel response (black, solid line) is processed by the algorithm and 11 taps are estimated before the threshold is reached. Those taps form a noise reduced equivalent channel.

In this case, when a new tap is found, we calculate the power that is left after removing all detected taps according to

$$P_{L+1} = \frac{1}{N} \sum_{n=1}^N \left(\mathbf{y}_n - \sum_{l=1}^{L+1} \alpha_l \cdot e^{j\phi_l} \cdot e^{-2\pi j \cdot m_l \cdot \nu_n} \right)^2 \quad (12)$$

When there are L taps above and the $(L+1)^{\text{st}}$ tap falls below threshold and it is provided that $|\mathbf{v}|^2 \sim \chi_2^2$, then we can set $\sigma = 2 \cdot P_{L+1}$ and stop the iterative estimation when

$$\alpha_{L+1}^2 < \underbrace{2 \cdot \sqrt{2 \cdot \log N}}_{=S} \cdot \frac{P_{L+1}}{N} \quad (13)$$

S is the threshold level and the additional factor $1/N$ comes from the time domain representation (8) while (12) is in frequency domain. Note that when (13) is fulfilled, the $(L+1)^{\text{st}}$ tap is not part of $\hat{\mathbf{h}}$. A flow chart of the iterative estimation algorithm is depicted in Fig. 6 and an example of the processed output can be seen in Fig. 7.

C. SNR estimation

The output of the iterative tap estimation can be used to denoise the measured data and to get an estimate of the SNR. We therefore calculate $\hat{\mathbf{h}}$ at the same pilot position as in the original channel (6). The effective SNR then notes

$$\begin{aligned} p^{(\text{equiv})} &= \frac{1}{N} \cdot \sum_{n=1}^N |\hat{\mathbf{h}}_n|^2 \\ p^{(\text{noise})} &= \frac{1}{N} \cdot \sum_{n=1}^N |\mathbf{y}_n - \hat{\mathbf{h}}_n|^2 \\ \text{SNR}_{\text{dB}} &\approx 10 \cdot \log_{10} \left(\frac{p^{(\text{equiv})} - \frac{3L}{2N} \cdot p^{(\text{noise})}}{(1 + \frac{3L}{2N}) \cdot p^{(\text{noise})}} \right) \quad (14) \end{aligned}$$

The factor $\frac{3L}{2N}$ accounts for the remaining noise which is proportional to the number of estimated taps.

D. Precision of the Capacity evaluation

The performance of the capacity evaluation procedure is evaluated here with an artificial keyhole channel as suggested by Gans et al. [11]. To obtain a keyhole channel matrix for a specific antenna pattern we first calculate n_t static Rayleigh fading channels $\mathbf{h}^{(K)}$ using $L^{(K)}$ taps for each channel. These channels represent the paths from the Tx to the keyhole. For the paths from the keyhole to the Rx we generate $L^{(S)}$ taps according to the static Rayleigh model. Each tap has the parameters α_l (amplitude), ϕ_l (phase) and m_l (normalized delay). In addition, we generate random values Φ_l (azimuth), Θ_l (elevation) for the angle of arrival and $p_l = [0, 1]$ for the polarization. So we get 6 parameters for each tap. Given an antenna pattern \mathbf{P}_r for receive element r in azimuth, elevation and polarization, we can calculate the FR $\mathbf{h}_r^{(S)}$ to

$$g_l = \alpha_l e^{j\phi_l} \cdot \left[\mathbf{P}_{r,\Phi,\Theta}^{(V)} \cdot p + \mathbf{P}_{r,\Phi,\Theta}^{(H)} \cdot (1-p) \right]$$

$$\mathbf{h}_{r,n}^{(S)} = \sum_{l=1}^{L^{(S)}} g_l \cdot e^{-2\pi j \cdot m_l \cdot \nu_n} \quad (15)$$

g_l is the complex amplitude with the antenna pattern applied. We get the keyhole matrix $\mathbf{H}^{(\text{kh})}$ for each carrier separately by calculating the Kronecker product

$$\mathbf{H}_n^{(\text{kh})} = \begin{pmatrix} \mathbf{h}_{1,n}^{(K)} \cdot \mathbf{h}_{1,n}^{(S)} & \cdots & \mathbf{h}_{n_t,n}^{(K)} \cdot \mathbf{h}_{1,n}^{(S)} \\ \vdots & \ddots & \vdots \\ \mathbf{h}_{1,n}^{(K)} \cdot \mathbf{h}_{n_r,n}^{(S)} & \cdots & \mathbf{h}_{n_t,n}^{(K)} \cdot \mathbf{h}_{n_r,n}^{(S)} \end{pmatrix} \quad (16)$$

The resulting links have $L = L^{(K)} \cdot L^{(S)}$ taps and the maximum excess delay is doubled due to product of the complex coefficients. We therefore need to limit m_l for all taps to $m_l < \frac{N}{2}$. In spatial domain, however, all matrices are singular. The algorithm for estimating the precision of the capacity

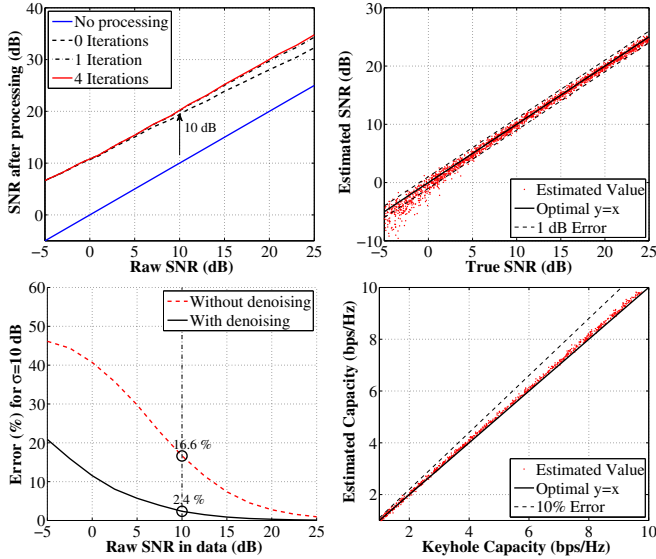


Figure 8. Results of the performance evaluation - Top left: the SNR after preprocessing vs. the raw SNR in the simulated data for a variable number of iterations; Top right: the performance of the SNR estimation; Bottom left: the relative error on the capacity calculation for a fixed $\sigma=10$ dB. Bottom right: the distribution of the predicted capacities.

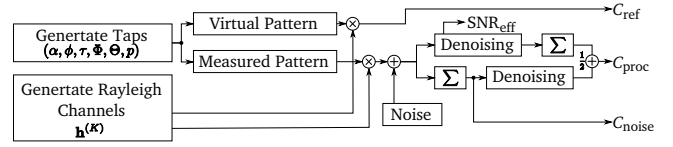


Figure 9. Algorithm for estimating the precision of the capacity calculation

calculation is depicted in Fig. 9. We first create keyhole channels for both, the measured and the virtual antenna. Then, the capacity C_{ref} is calculated from the 2x2 response of the virtual antenna. This value serves as a reference. The response of the measured array is further processed by adding AWGN, weighting, summing up the channels and denoising.

Initial tests on the measurement data show that the radio channel has up to 36 taps, so we set the simulation accordingly. Results are depicted in Fig. 8. The SNR is increased by approximately 10 dB when using 4 iterations in the tap estimation. Effective SNRs are predicted with a standard deviation of 0.45 dB for values above 0 dB. Estimating the capacity at the measurement SNR without denoising produces an error of 16% on the Keyhole channel. This error can be bounded below 3% when using the denoising procedure.

ACKNOWLEDGMENTS

The authors wish to thank the German Ministry of Education and Research (BMBF) for financial support in the national collaborative project EASY-C under contract number 01BU0631. Furthermore we thank our partners Actix, Alcatel-Lucent, Deutsche Telekom, Ericsson, HHI, Kathrein, Qualcomm, TU Dresden and Vodafone for financial support of the campaign in Dresden. Many thanks to C. Schneider, G. Sommerkorn (all from TU Ilmenau) and S. Warzügel (MEDAV) for assistance during the measurements and M. Schellmann from HHI and M. Käske from TU Ilmenau for the fruitful discussions.

REFERENCES

- [1] I. E. Telatar, "Capacity of multi-antenna gaussian channels," *Europ. Trans. Telecommun.*, vol. 10, no. 6, pp. 585–596, 1999.
- [2] D. Chizhik, J. Ling, P. Wolniansky, R. Valenzuela, N. Costa, and K. Huber, "Multiple-input-multiple-output measurements and modeling in Manhattan," *IEEE J. Sel. Areas Commun.*, vol. 21, pp. 321–331, 2003.
- [3] V. Jungnickel, S. Jaeckel, L. Thiele, L. Jiang, U. Krüger, A. Brylka, and C. Helmolt, "Capacity measurements in a cooperative multicell MIMO network," *IEEE Trans. Veh. Technol.*, vol. 58, pp. 2392–2405, 2009.
- [4] A. Richter, "Estimation of radio channel parameters: Models and algorithms," Ph.D. dissertation, Technische Universität Ilmenau, 2005.
- [5] R. Thomä, D. Hampicke, A. Richter, G. Sommerkorn, and U. Trautwein, "MIMO vector channel sounder measurement for smart antenna system evaluation," *Europ. Trans. Telecommun.*, vol. 12, pp. 427–438, 2001.
- [6] S. Jaeckel, L. Thiele, A. Brylka, L. Jiang, and V. Jungnickel, "Intercell interference measured in urban areas," *Proc. IEEE ICC '09*, 2009.
- [7] D. L. Donoho and I. M. Johnstone, "Ideal denoising in an orthonormal basis chosen from a library of bases," *Comptes Rendus Acad. Sci., Ser. I*, vol. 319, pp. 1317–1322, 1994.
- [8] —, "Ideal spatial adaptation by wavelet shrinkage," *Biometrika*, vol. 81, pp. 425–455, 1994.
- [9] D. Tse and P. Viswanath, *Fundamentals of Wireless Communication*. Cambridge University Press, 2005.
- [10] E. Candes and T. Tao, "The dantzig selector: Statistical estimation when p is much larger than n ," *Ann. Statist.*, vol. 35, pp. 2313–2351, 2007.
- [11] M. Gans, N. Amitay, and Y. Yeh, "Outdoor BLAST measurement system at 2.44 GHz: Calibration and initial results," *IEEE J. Sel. Areas Commun.*, vol. 20, no. 3, pp. 570–583, 2002.